AAPS PharmSciTech (2024) 25:103
https://doi.org/10.1208/s12249-024-02809-7

RESEARCH ARTICLE

Implications of Low-concentration Polymer on the Physical Stability of Glassy Griseofulvin: Role of the Segmental Mobility

Yanan Wang[1,3] · Chai-Yee Chin[2] · Naveen Kumar Hawala Shivashekaregowda[2,3] · Qin Shi[1]

Received: 30 January 2024 / Accepted: 17 April 2024

Abstract

Crystallization of amorphous pharmaceutical solids are widely reported to be affected by the addition of polymer, while the underlying mechanism require deep study. Herein, crystal growth behaviors of glassy griseofulvin (GSF) doped with various 1% *w/w* polymer were systematically studied. From the molecular structure, GSF cannot form the hydrogen bonding interactions with the selected polymer poly(vinyl acetate), polyvinyl pyrrolidone (PVP), 60:40 vinyl pyrrolidone-vinyl acetate copolymer (PVP/VA 64), and poly(ethylene oxide) (PEO). 1% *w/w* polymer exhibited weak or no detectable effects on the glass transition temperature (T_g) of GSF. However, crystal growth rates of GSF was altered from 4.27-fold increase to 2.57-fold decrease at 8 ℃ below T_g of GSF. Interestingly, the ability to accelerate and inhibit the growth rates of GSF crystals correlated well with T_g of polymer, indicating the controlling role of segmental mobility of polymer. Moreover, ring-banded growth of GSF was observed in the polymer-doped systems. Normal compact bulk and ring-banded crystals of GSF were both characterized as the thermodynamically stable form I. More importantly, formation of ring-banded crystals of GSF can significantly weaken the inhibitory effects of polymer on the crystallization of glassy GSF.

Keywords banding morphology · crystal growth · flory–huggins interactions · griseofulvin · physical stability

Introduction

With the success in drug discovery, increasing number of new candidates and chemical entities have suffered the problems of poor water solubility [1]. One of the promising techniques for enhancing solubility and dissolution is to use the amorphous form [2–4]. Compared to their crystalline counterparts, amorphous drugs exhibit superior properties in solubility, dissolution, and drug delivery [5]. However, due to their higher energy, amorphous drug tends to crystallize, thus losing its advantages in solubility and dissolution [6, 7]. Maintaining the stability of amorphous drugs and avoiding the possible physicochemical changes is important to fulfill the roles of these applications. Therefore, understanding the mechanisms of crystallization is crucial to develop robust amorphous pharmaceutical formulations.

Crystallization consists of two key processes, i.e., nucleation and crystal growth. Crystal nucleation has been widely explored in several fields of science and remains significant questions [8]. For one-component liquid system, crystal growth above T_g can be considered as a result of the co-action of molecular diffusion and thermodynamic driving force. With increasing in supercooling, molecular diffusion gradually plays the controlling role for crystal growth process, as evidenced by the approximately same temperature dependences of the measured self-diffusion coefficients and crystal growth rates [9, 10]. According to this molecular diffusion-controlled theory, crystal growth in glassy state should extremely slow. However, some organic glasses have been reported to show much faster crystal growth behaviors blow or near T_g than those predictions by diffusion-controlled models [11–14]. For instance, glass-to-crystal (GC) growth, reported in some organic small-molecules or co-amorphous systems, can be activated as decreasing the temperature near or below

✉ Naveen Kumar Hawala Shivashekaregowda
navigcp@gmail.com

✉ Qin Shi
12127@jsmc.edu.cn

1 School of Pharmacy, Jiangsu Vocational College of Medicine, Yancheng 224005, China

2 School of Pharmacy, Faculty of Health and Medical Science, Taylor's University, Subang Jaya 47500, Malaysia

3 Digital Health and Medical Advancement Impact Lab, Taylor's University, Subang Jaya, Selangor 47500, Malaysia

Published online: 07 May 2024

T_g [15–18]. GC growth was initially observed in o-terphenyl in 1967 and has been reported in over 20 organic systems [18]. Recent studies also reported that crystal growth of amorphous drug can be affected by the addition of the polymer [19–28]. Implications of polymer on the crystal growth of amorphous drug have been explained by several mechanisms including the polymer segmental mobility [19, 29], polymer enrichment [26, 27], drug-polymer molecular interactions [30–32].

Griseofulvin is a model system for investigating the crystallization of amorphous solids. This study compared four polymer additives as the accelerator and inhibitor of GC growth of griseofulvin. 1% *w/w* polymers were selected to ensure that these polymers can exist in dilute solution and little effects on T_g of griseofulvin. The selected polymers were PVP, PVAc, PEO, and PVP/VA 64. From the perspective of molecular structure, these selected polymers cannot form the hydrogen bonding interactions with griseofulvin. Interestingly, ring-banded growth was also observed in GSF system doped with low-concentration polymer.

Materials and Methods

Materials

GSF was purchased from J&K Scientific Co. Ltd. PVP K12, PVP K17, PVP K25, PVP K90, and PVP/VA 64 were purchased from BASF. PVAc was purchased from Scientific Polymer Products Inc. PEO was obtained from Sigma-Aldrich. Molecular structure of used polymer and GSF was shown in Fig. 1. Table I shows the T_{gs} of the selected polymer.

Table I *Tg* The Selected Polymer in Present Study

Polymer	T_g (℃)
PVP K12	102
PVP K17	130
PVP K25	155
PVP K90	178
PVAc	36
PEO100000	-47
PVPVA64	102

Preparation of Polymer-doped GSF Mixtures

Polymer-doped GSF mixture was prepared by cryogenic-milling method, one method widely reported to facilitate the uniform drug-polymer binary systems. GSF systems containing 10% *w/w* polymer were prepared by mechanically blending 0.1 g polymer and 0.9 g pure crystalline GSF at 10 Hz for 5 cycles by using liquid nitrogen as the coolant. Subsequently, for preparing the GSF mixture doped with 1% polymer, these resulting mixtures were further with GSF with a molar ratio of 1:9.The times of milling and cool-down process was 2 min.

Thermal Analysis

Thermodynamic properties of pure and polymer-doped GSF systems were examined by using a TA Discovery 250 DSC under 50 mL/min N_2 purge. These samples were firstly heated up to 220 ℃ and anneal for 3 min for completely melting. Subsequently, these samples were cooled to 0 ℃ at a cooling rate of 20 ℃ min^{-1} to obtain amorphous GSF and polymer-doped GSF systems. The heating rate used in the experiments is 10 ℃ min^{-1}.

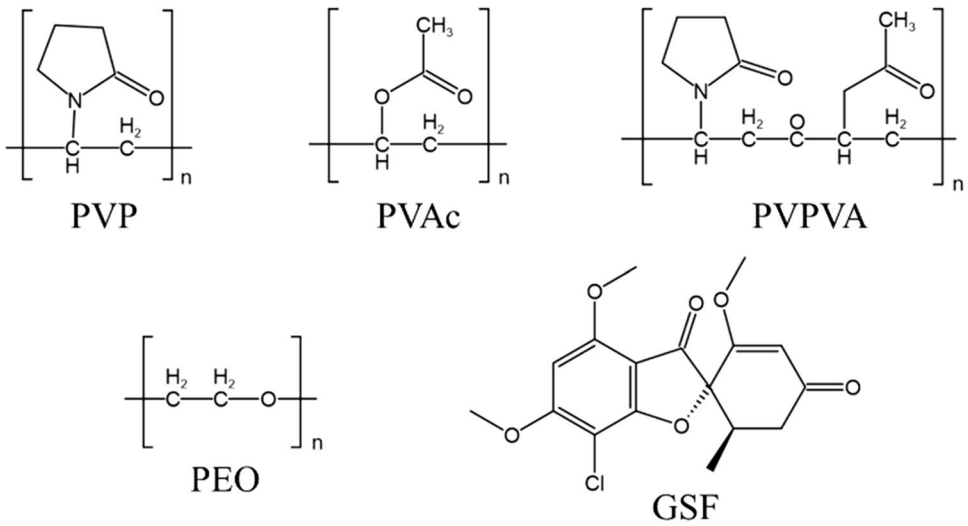

Fig. 1 Molecular structure of used polymer and GSF

Solubility Measurement of GSF Crystals in Polymer

Solubility of GSF in polymer was measured by an annealing method [33, 34]. Approximately 12 mg of GSF/polymer (30/70, 50/50, 70/30, 90/10, *w/w* ratio) physical mixtures were sealed hermetically in an aluminum pans. Subsequently, these mixtures were annealed at the desired temperature for 4 h. After the annealing process, these samples were further scanned to check whether residual crystals remained with a 10℃/min heating rate. The solubility temperature was measured as the disappearance of the melting peak, and thus facilitating further determining the miscibility between GSF and polymer based on Flory–Huggins theory.

Raman Microscopy

Polymorphs of GSF in pure or polymer-doped systems were identified by a Raman microscopy (ThermoFisher DXR) equipped with a 780 nm laser. A 50 X objective was used and laser power is ~ 20 mW. Spectra was obtained by using exposure time of 2 s by 30 times.

Crystal Morphologies and Growth Kinetics of GSF Doped with 1% *w/w* Polymer

Crystal morphologies and growth kinetics of GSF in the presence of 1% *w/w* polymer was tracked by using polarized light microscope equipped with a KELX-4A hot stage. Approximately 4 mg polymer-doped GSF was initially melt between two round coverslips (15 mm diameter) and subsequently quench to room temperature. As evidenced by the absence of birefringence, the melt-quenched polymer-doped GSF samples were confirmed to be amorphous. To obtain the crystal morphologies and growth kinetics of GSF crystals, these prepared samples were placed on the hot stage at 80℃. GSF form I can crystallize spontaneously from the edge of the glassy samples. Growth rates of GSF crystals were measured by tracking advancing speed of crystals in the interior. The reported growth rates were the average of three independent measurements.

Powder X-ray Diffraction (PXRD)

PXRD of GSF was performed by a powder X-ray diffractometer (D8 Advance, Bruker, Germany) at room temperature. A X-ray diffractometer with Cu Kα radiation (40 kV × 40 mA) was used. The scan was measured over the angular range of 3–40° at the step speed of 0.02° with a 1 s dwell time. Prior to PXRD experiments, one cover glass was detached from the bulk samples to expose GSF crystals. Then the PXRD data were collected from banding growth form of GSF crystals.

Results and Discussions

Morphologies of GSF Crystals in Pure and Polymer-doped Systems

GSF, one well-studied polymorphic drug, is a classical system for studying the crystallization of amorphous formulations [35–39]. In addition to the thermodynamic stable polymorph (Form I), crystal structure of its two metastable polymorphs (Form II, Form III) have also been reported in very recent studies *via* melt crystallization [38, 40]. Figure 2 showed the morphologies of GSF in pure and 1% *w/w* polymer-doped systems at 80 ℃ (8 ℃ below T_g

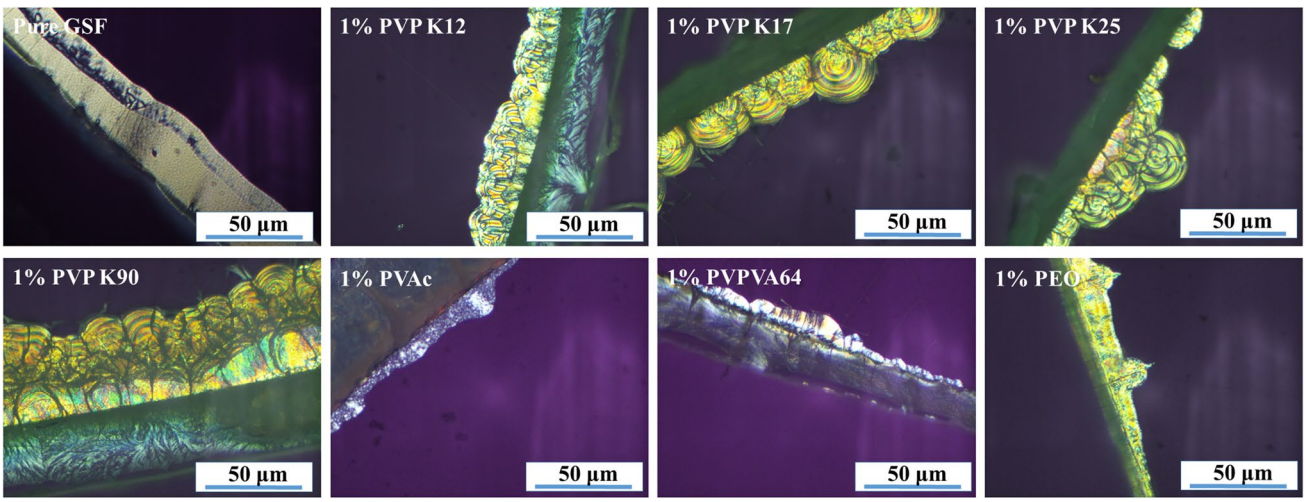

Fig. 2 Growth morphologies of GSF crystals grown pure and 1% *w/w* polymer-doped systems at 80 ℃

of pure GSF). Pure GSF grew as compact spherulites (GC growth) at 80 ℃ with a fine-grained structure. Powell *et al.* reported that crystals of o-terphenyl (OTP) grown in glassy state were compared of grains ~ 500 nm in size [17]. They proposed that GC growth was most likely to be an assembly of crystalline domains, which were separated by small voids [17]. Our results further supported the view that GC growth was facilitated by the surface. Herein, GC growth was proposed to be a process steadily created free surface by fracture, facilitating local crystal growth [17]. For the polymer doped systems, some of GSF crystals can also grow as normal compact spherulite. For comparisons, partial crystals of GSF in the presence of polymer exhibited ring-banded morphologies.

Figure 3 exhibited Raman spectra of GSF crystals grew in pure and 1% *w/w* polymer-doped systems at 80 ℃. Fingerprint regions (wavenumber range of 500–1800 cm^{-1}) in Raman spectra were widely used for identifying polymorphism [41]. In previous study, Su *et al.* successfully obtained the Raman spectra of GSF polymorphs [38]. Compared to the form I, form II and III of GSF exhibited different Raman peaks at 1750–1550 cm^{-1} and 1300–900 cm^{-1}. Herein, GSF crystals grew in pure or polymer-doped systems were all identified as form I.

Mixing State of Polymer-doped GSF Systems

Investigation of the miscibility between GSF and polymer at the used concentration of 1% *w/w* was important for understanding polymer effects on the crystal growth process. Liquid drops of polymer-doped liquid GSF were optically clear and homogeneous, indicating that polymer can be uniformly dispersed in GSF. Miscibility of GSF-polymer mixture was further evidenced by single T_g of system, exhibiting no signals of phase separation.

Measurement of Flory–Huggins interaction parameter (χ) facilitated the understanding of the mixing state of drug-polymer binary systems [42–44]. In our previous study, a small negative value of χ ~—0.29 was reported for GSF/PEO system, indicating the miscibility between GSF and PEO [45]. In the present study, Flory–Huggins interaction parameters of other binary systems (GSF-PVP, GSF-PVAc, GSF-PVPVA 64) were also calculated on the basis of the obtained solubility data of GSF in PVP, PVAc, or PVPVA 64. Herein, the following equation was used for calculating the activity *a* of GSF.

$$\ln a = (\Delta H_m/\mathrm{R})\left(\frac{1}{T_m} - \frac{1}{T}\right) \quad (1)$$

where T_m was melting point of GSF while ΔH_m was the enthalpy of T_m. Herein, the measure T_m of GSF form I is ~ 218.8℃ and the measured ΔH_m is ~ 116 J/g. *T* represented the temperature at which GSF solubility in polymer was measured, equivalent to depressed T_m. As shown in Fig. 4, Activity *a* of GSF decreased with the increasing PVP K12 weight fraction in the systems. As evidenced by the red line of Flory–Huggins fits, *a* of GSF in PVP K12

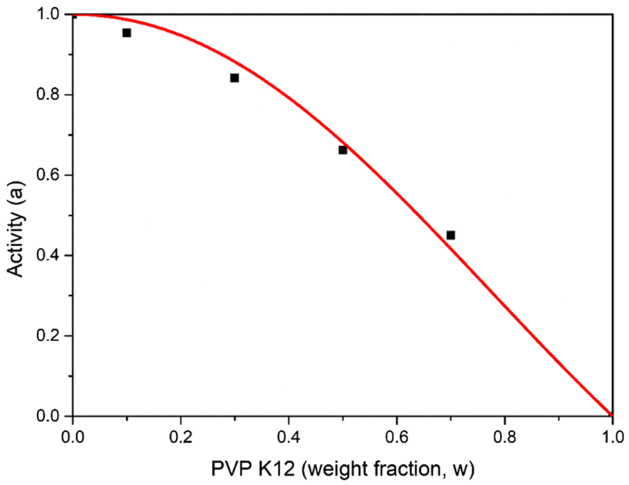

Fig. 4 Activity of GSF as a function of weight fraction of PVP K12

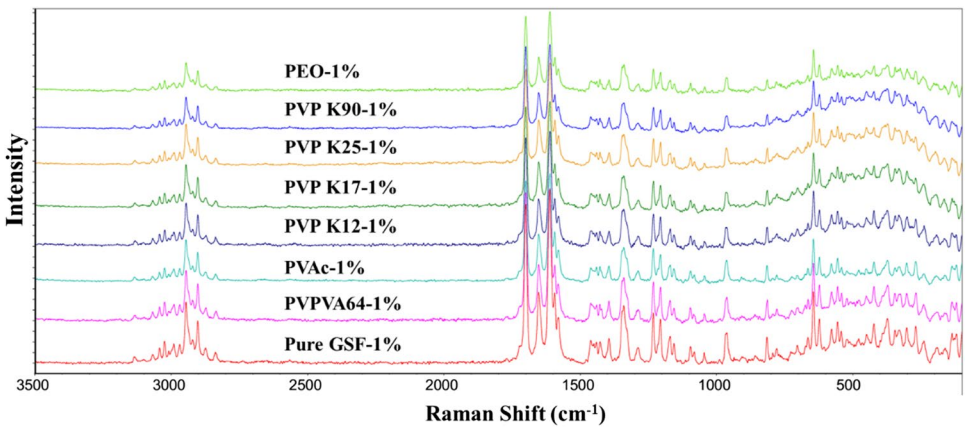

Fig. 3 Raman spectra of GSF system in pure and 1% *w/w* polymer-doped systems at 80 ℃

Table II Value of χ for GSF-polymer Systems

Systems	Value of χ
GSF-PVP K12	-0.75 (±0.06)
GSF-PVP K17	-0.39 (±0.11)
GSF-PVP K25	-0.78 (±0.13)
GSF-PVP K90	-0.71 (±0.18)
GSF-PVAc	-0.05 (±0.02)
GSF-PEO100000	-0.28 (±0.04)
GSF-PVPVA64	-0.91 (±0.05)

were well fitted to Flory–Huggins model. Activity a of GSF in PVP, PVAc, PVPVA 64 can be described by the following equation according to Flory–Huggins theory.

$$\ln a = \ln v_{drug} + (1 - r)v_{polymer} + \chi v_{polymer}^2 \quad (2)$$

where v_{drug} and $v_{polymer}$ respectively represented volume fractions of drug and polymer. Herein, the volume fraction was simplified as the weight fractions. The parameter r represented the ratio of drug-polymer molecular weight.

Table II showed the values of Flory–Huggins parameters χ for GSF-polymer systems in present work. Flory–Huggins interaction parameters χ of all these drug-polymer systems exhibited the small negative value. These results suggested that GSF can be miscible with selected polymer from the thermodynamic perspective. Yu and the coworkers measured the Flory–Huggins parameters χ of indomethacin and nifedipine in PVP, PVPVA, and PVAc [33]. Compared to GSF-polymer systems, Flory–Huggins parameters of indomethacin-polymer and nifedipine-polymer systems exhibited more negative value. In our previous study, we compared the decrease extent in the activities of three drugs in PEO [34]. Drug-polymer miscibility followed the order as indomethacin > nifedipine > GSF [34]. GSF contains the hydrogen bonding acceptor while no hydrogen bonding donor. Polymer used in present work contains no hydrogen bonding donors. It was inferred that no hydrogen bonding interactions can be existed in these systems. For comparison, indomethacin and nifedipine was able to form the hydrogen bonding interactions with these polymers. These results indicated that stronger drug-polymer molecular interactions might lead to more negative values of Flory–Huggins interaction parameters

Crystal Growth Kinetics

Figure 5 showed the growth rates of GSF in 1% *w/w* polymer-doped system at 80 ℃. Crystal growth of GSF can be effectively altered by these polymer additives. For instance, 1% *w/w* PVP 90 yielded a 2.57-fold reduction in crystal growth rate. For comparisons, crystal growth rate of GSF

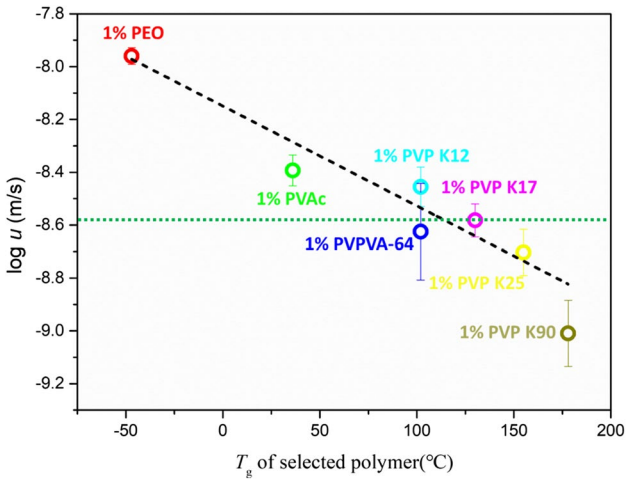

Fig. 5 Normal bulk growth kinetics of GSF crystals in 1% polymer-doped systems at 80 ℃ (T_g- 8 ℃). Green dashed line represents the growth rates of pure GSF at 80 ℃

can be increased by 4.27-fold by the addition of 1% *w/w* PEO. More importantly, the inhibiting and accelerating effects of polymer on crystal growth correlated well with the T_g of the used polymer. From the perspective of Flory–Huggins theory, drug-polymer molecular interactions in these systems were similar. These results suggested that segmental mobility of polymer can be a key factor for affecting the crystal growth of glassy GSF. Powell *et al.* reported similar results in glassy nifedipine doped with 1% *w/w* polymer [19]. Crystal growth rates of glassy nifedipine can be altered by the addition of low-concentration polymer [19]. Herein, the inhibitory effects of polymer on crystal growth of nifedipine also correlated well with the T_g of the used polymer [19]. No evidences were observed between the inhibitory effects of polymer and the strength of drug-polymer hydrogen bonding interactions [19].

Huang *et al.* found that effects of polymer on crystal growth kinetics can form an interesting master curve in the variable $(T_{g,\,polymer}\text{-}T_{g,host})/T_{crystal}$ [29]. Herein, $T_{crystal}$ represented the crystallization temperature. They proposed that segmental mobility of polymer relative to the host-molecule dynamics was the controlling factors for affecting the crystal growth [29]. It was expected that local polymer-rich regions would be created at the crystal growth front *via* the polymer rejected from the drug crystals. Host molecules should pass through these regions during crystal growth process [29]. In these polymer-rich regions, segmental mobility of polymer was expected to affect the traversed rates of host molecules. This view was strongly supported by the findings in recent studies focusing on PEO effects on the crystallization of amorphous drugs [24, 34, 45]. Significant accelerating effects of low-concentration PEO on crystal growth cannot be fully explained by

the increased global mobility [24]. Zhang *et al.* proposed crystal growth in the presence of polymer can be both affected by the molecular mobility and interfacial free energy between crystal and melt [25]. More importantly, recent studies provided the direct experimental evidence for the existence of polymer enrichment at the crystal-melt interface during crystal growth process [26, 27].

In present study, in addition to PEO, the rest polymer (1% *w/w*) exhibited weak effects on system T_g. However, significant changes were observed in the crystal growth kinetics of GSF doped with these polymers. For instance, 1% *w/w* PVP K90 yielded a 2.57-fold decrease in the growth rates of GSF at 80℃ ($T_{g,GSF}$-8℃). For comparisons, same content of PVP K90 was reported to exhibit a tenfold reduction on the crystal growth rates of nifedipine at 30℃ ($T_{g,NIF}$-12℃) [19]. According to the master curve proposed by Huang *et al.*, the different effects of PVP K90 on GSF and nifedipine were mainly attributed to different host-molecule dynamics. Sato *et al.* also proposed that differences in the drug and polymer molecular mobility also affected the crystal growth in these binary systems [20]. GSF exhibits a relative higher T_g at 88 ℃ while nifedipine has a relative lower T_g at 42 ℃. 1% *w/w* PEO-doped GSF and nifedipine systems is expected to exhibit the different host-molecule dynamics, which can explain the better accelerating effects of PEO in GSF in comparison with that in nifedipine. 1% PEO can accelerate the growth rate of GSF by 4.27-fold at 80℃ ($T_{g,GSF}$-8℃). However, only 30% increase of crystal growth rates can be observed for nifedipine at 30℃ ($T_{g,NIF}$-12℃) doped with 1% *w/w* PEO. In addition, slight or negligible changes in the T_g and global mobility of GSF system cannot be sufficient to support the obvious accelerating or inhibiting effects of polymer. Our results supported the view that crystal growth in polymer-based amorphous systems was both governed by local polymer enrichment and global system mobility.

In the past decades, drug-polymer specific interactions were also demonstrated to be a main factor for inhibiting the crystallization of amorphous drug [6, 46, 47]. Strength and extensiveness of hydrogen bonding interactions were reported to correlate well with the extent of decrease in crystal growth [46, 47]. In present study, GSF cannot form the hydrogen bonding interactions with the selected polymer from the perspective of molecular structure. The reduced crystal growth of GSF by polymer was proposed to be mainly attributed to their low segmental mobility rather than the drug-polymer interactions. In addition, it should be noted that our work focused on the effects of polymers on crystal growth in glassy state. For comparisons, Taylor and co-workers mainly focused on the effects of polymers on the crystal growth in supercooled liquid. The differs in the experimental temperature range, representing the differ in crystal growth mechanisms, was perhaps responsible for different mechanisms for explaining the role of polymer.

Banding Growth

As above-mentioned, GSF can grow in the banding spherulites when doped with low-concentration polymer. We carefully collected the samples of banding crystals of GSF grown in the interior and obtained the PXRD results. As shown in Fig. 6, these banding crystals of GSF were identified as the form I, as compared to the calculated XRD patterns from the crystal structure of GSF polymorphs. Raman spectra of banding and normal bulk crystal were also identified to be form I (Fig. 7b). Banded spherulites were first observed in the crystals of chalcedony, showing the fibrous form of quartz [48]. Banded spherulites can be the radial organization of fibrous or plank-like crystals. In addition, concentric rings of varying linear birefringence can also be observed under the petrographic microscope for these banded patterns [48]. These polycrystalline patterns have been widely reported in organic molecular crystals, high polymer, simple salts, etc [48–51]. It is proposed that helical twisting of thin lamellae or fibers were responsible for oscillating variation of optical properties [48–51]. From the perspective of the crystallographic data of GSF form I, the crystal lattice can be approximately considered as thin lamellae [38]. It was proposed that the addition of 1% *w/w* PVP K90 might participate into the crystal growth process, and thus facilitating helical twisting of thin lamellae of GSF crystals. We also compared the crystal growth kinetics of GSF doped with 1% *w/w* PVP K90 for both the banding form and normal compart spherulite. Another interesting finding was that the inhibitory effects of PVP K90 can be weakened as the formation of banding growth (Fig. 7a). Compared to normal bulk growth, banding growth of GSF exhibited a much faster rate.

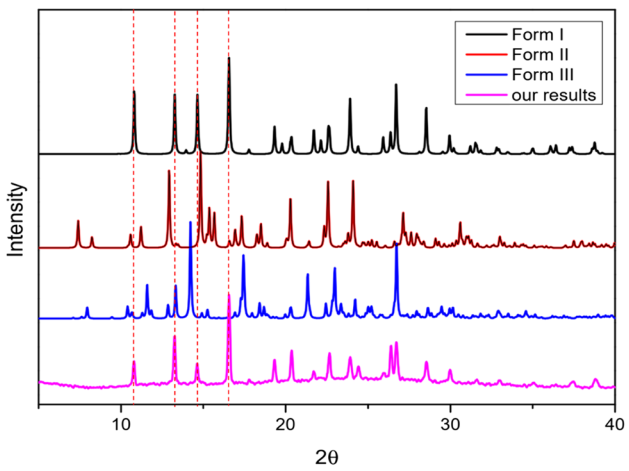

Fig. 6 PXRD results of banding crystals of GSF doped with 1% *w/w* PVP K90 and the calculated XRD patterns from crystal structure of GSF form I, II, and III

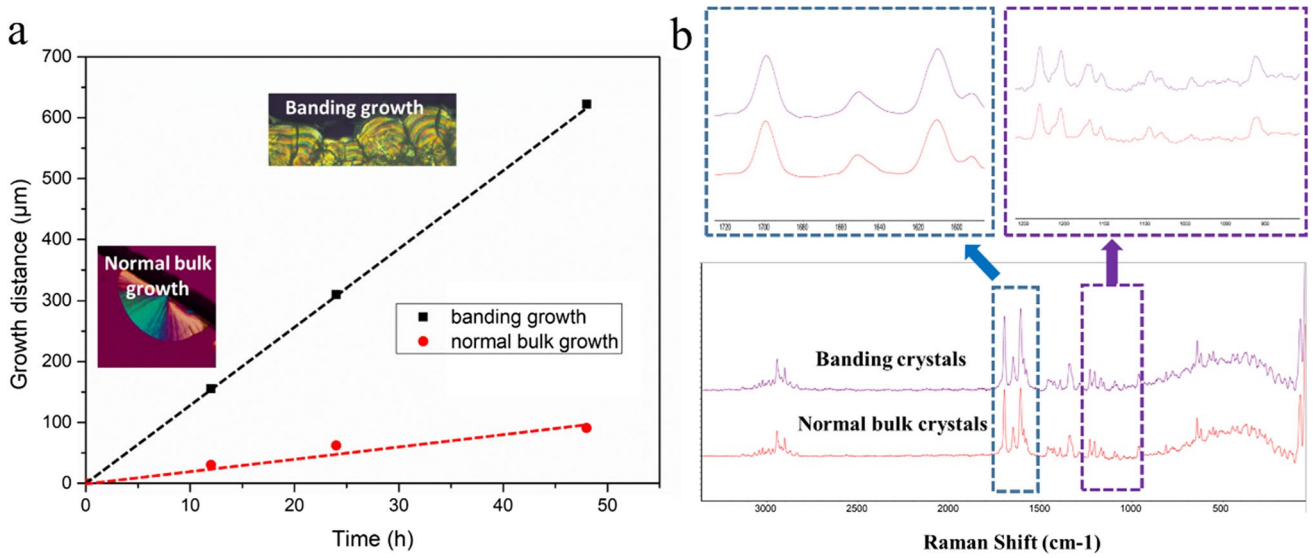

Fig. 7 **a** Crystal growth of 1% w/w PVP K90-doped GSF in the banding form and normal compart spherulite. The inset is the morphology of banding and normal bulk growth in the same samples. **b** Raman spectra of normal bulk and banding crystals of griseofulvin in the presence of 1% PVP K90

Conclusion

In this work, we reported that growth kinetics of GSF crystals were affected by the addition of low-concentration polymer in the glassy state. Inhibiting or accelerating effects of polymer on crystal growth of GSF correlated well with polymer T_g, supporting the control role of segmental mobility of polymer. Interestingly, the addition of polymer also induced banding growth in glassy GSF. Moreover, the growth inhibition effects of polymer were substantially reduced as the formation of banding growth. These results are important for further understanding the implications of polymer on the crystal growth behaviors of amorphous pharmaceutical solids.

Acknowledgements The authors are grateful for the financial support of this work by Natural Science Foundation of Jiangsu Province (No.BK20211114), Medical General Projects of Jiangsu Commission of Health (No. H2023070), Scientific and Technological Innovation Team Project of Jiangsu Vocational College of Medicine (grant No. 20234302), Key Medical Research Projects of Health Commission of Yancheng (No. YK2023031), Excellent Teaching Team of "Qinglan Project" in Jiangsu Province (2023), and Jiangsu Higher Education Institution Innovative Research Team for Science and Technology (2023).

Author Contributions **Yanan Wang**: Methodology, Writing-original draft. **Chai-Yee Chin**: Writing-review & editing. **Naveen Kumar Hawala Shivashekaregowda**: Resources, Supervision, Writing-review & editing. **Qin Shi**: Funding acquisition, Conceptualization Resources, Supervision, Writing-original draft.

Data Availability All the data represented the result are available as a part of this article and not additional source data are required.

Declarations

Conflict of Interest The authors declare no competing financial interests.

References

1. Kalepu S, Nekkanti V. Insoluble drug delivery strategies: review of recent advances and business prospects. Acta Pharm Sin B. 2015;5:442–53.
2. Yu L. Amorphous pharmaceutical solids: preparation, characterization and stabilization. Adv Drug Deliv Rev. 2001;48:27–42.
3. Vasconcelos T, Marques S, das Neves J, Sarmento B. Amorphous solid dispersions: Rational selection of a manufacturing process. Adv Drug Deliv Rev. 2016;100, 85–101.
4. Shi Q, Li F, Yeh S, Moinuddin SM, Xin J, Xu J, Chen H, Ling B. Recent advances in enhancement of dissolution and supersaturation of poorly water-soluble drug in amorphous pharmaceutical solids: A review. AAPS PharmSciTech. 2021;23:16.
5. Zhang J, Guo M, Luo M, Cai T. Advances in the development of amorphous solid dispersions: The role of polymeric carriers. Asian J Pharm Sci. 2023;18:100834.
6. Shi Q, Li F, Yeh S, Wang Y, Xin J. Physical stability of amorphous pharmaceutical solids: Nucleation, crystal growth, phase separation and effects of the polymers. Int J Pharm. 2020;590:119925.
7. Sun Y, Zhu L, Wu T, Cai T, Gunn EM, Yu L. Stability of amorphous pharmaceutical solids: crystal growth mechanisms and effect of polymer additives. AAPS J. 2012;14:380–8.
8. Sosso GC, Chen J, Cox SJ, Fitzner M, Pedevilla P, Zen A, Michaelides A. Crystal nucleation in liquids: Open questions and future challenges in molecular dynamics simulations. Chem Rev. 2016;116(12):7078–116.
9. Swallen SF, Ediger MD. Self-diffusion of the amorphous pharmaceutical indomethacin near Tg. Soft Matter. 2011;7:10339–44.

10. Mapes MK, Swallen SF, Ediger MD. Self-diffusion of supercooled o -terphenyl near the glass transition temperature. J Phys Chem B. 2006;110:507–11.
11. Wang K, Sun CC. Crystal growth of celecoxib from amorphous state: Polymorphism, growth mechanism, and kinetics. Cryst Growth Des. 2019;19:3592–600.
12. Shi Q, Tao J, Zhang J, Su Y, Cai T. Crack- and bubble-induced fast crystal growth of amorphous griseofulvin. Cryst Growth Des. 2019;20:24–8.
13. Shi Q, Wang Y, Xu J, Liu Z, Chin C. Fast crystal growth of amorphous nimesulide: implication of surface effects. Acta Cryst B. 2022;78:33–9.
14. Chen A, Cai P, Luo M, Guo M, Cai T. Melt crystallization of celecoxib-carbamazepine cocrystals with the synchronized release of drugs. Pharm Res. 2023;40:567–77.
15. Shi Q, Cai T. Fast crystal growth of amorphous griseofulvin: Relations between bulk and surface growth modes. Cryst Growth Des. 2016;16:3279–86.
16. Powell CT, Paeng K, Chen Z, Richert R, Yu L, Ediger MD. Fast crystal growth from organic glasses: comparison of o-terphenyl with its structural analogs. J Phys Chem B. 2014;118:8203–9.
17. Powell CT, Xi H, Sun Y, Gunn E, Chen Y, Ediger MD, Yu L. Fast crystal growth in o-terphenyl glasses: A possible role for fracture and surface mobility. J Phys Chem B. 2015;119:10124–30.
18. Shi Q, Moinuddin SM, Wang Y, Ahsan F, Li F. Physical stability and dissolution behaviors of amorphous pharmaceutical solids: Role of surface and interface effects. Int J Pharm. 2022;625:122098.
19. Powell CT, Cai T, Hasebe M, Gunn EM, Gao P, Zhang G, Gong Y, Yu L. Low-concentration polymers inhibit and accelerate crystal growth in organic glasses in correlation with segmental mobility. J Phys Chem B. 2013;117:10334–41.
20. Sato T, Taylor LS. Acceleration of the crystal growth rate of low molecular weight organic compounds in supercooled liquids in the presence of polyhydroxybutyrate. CrystEngComm. 2017;19:80–7.
21. Schram CJ, Beaudoin SP, Taylor LS. Impact of polymer conformation on the crystal growth inhibition of a poorly water-soluble drug in aqueous solution. Langmuir. 2015;31:171–9.
22. Schram CJ, Taylor LS, Beaudoin SP. Influence of polymers on the crystal growth rate of felodipine: Correlating adsorbed polymer surface coverage to solution crystal growth inhibition. Langmuir. 2015;31:11279–87.
23. Shi Q, Chen H, Wang Y, Wang R, Xu J, Zhang C. Amorphous solid dispersions: Role of the polymer and its importance in physical stability and in vitro performance. Pharmaceutics. 2022;14:1747.
24. Shi Q, Zhang J, Zhang C, Jiang J, Tao J, Zhou D, Cai T. Selective acceleration of crystal growth of indomethacin polymorphs by low-concentration poly(ethylene oxide). Mol Pharm. 2017;14:4694–704.
25. Zhang S, Britten JF, Chow AHL, Lee TWY. Impact of crystal structure and polymer excipients on the melt crystallization kinetics of itraconazole polymorphs. Crys Growth Des. 2017;17:3433–42.
26. Zhang J, Shi Q, Tao J, Peng Y, Cai T. Impact of polymer enrichment at the crystal-liquid interface on crystallization kinetics of amorphous solid dispersions. Mol Pharm. 2019;16:1385–96.
27. Zhang J, Shi Q, Guo M, Liu Z, Cai T. Melt crystallization of indomethacin polymorphs in the presence of poly(ethylene oxide): Selective enrichment of the polymer at the crystal-liquid interface. Mol Pharm. 2020;17:2064–71.
28. Zhang J, Liu Z, Wu H, Cai T. Effect of polymeric excipients on nucleation and crystal growth kinetics of amorphous fluconazole. Biomater Sci. 2021;9:4308–16.
29. Huang C, Powell CT, Sun Y, Cai T, Yu L. Effect of low-concentration polymers on crystal growth in molecular glasses: A controlling role for polymer segmental mobility relative to host dynamics. J Phys Chem B. 2017;121:1963–71.
30. Kothari K, Ragoonanan V, Suryanarayanan R. The role of drug-polymer hydrogen bonding interactions on the molecular mobility and physical stability of nifedipine solid dispersions. Mol Pharm. 2015;12:162–70.
31. Mistry P, Suryanarayanan R. Strength of drug-polymer interactions: Implications for crystallization in dispersions. Cryst Growth Des. 2016;16:5141–9.
32. Sahoo A, Kumar NSK, Suryanarayanan R. Crosslinking: An avenue to develop stable amorphous solid dispersion with high drug loading and tailored physical stability. J Contr Release. 2019;311–312:212–24.
33. Sun Y, Tao J, Zhang GG, Yu L. Solubilities of crystalline drugs in polymers: an improved analytical method and comparison of solubilities of indomethacin and nifedipine in PVP, PVP/VA, and PVAc. J Pharm Sci. 2010;99:4023–31.
34. Shi Q, Cheng J, Li F, Xu J, Zhang C. Molecular mobility and crystal growth in amorphous binary drug delivery systems: Effects of low-concentration poly(ethylene oxide). AAPS PharmSciTech. 2020;21:317.
35. Huang C, Ruan S, Cai T, Yu L. Fast surface diffusion and crystallization of amorphous griseofulvin. J Phys Chem B. 2017;121:9463–8.
36. Li F, Xin J, Shi Q. Diffusion-controlled and `diffusionless' crystal growth: relation between liquid dynamics and growth kinetics of griseofulvin. J Appl Crystallogr. 2021;54:142–7.
37. Petersen AB, Rønnest MH, Larsen TO, Clausen MH. The chemistry of griseofulvin. Chem Rev. 2014;114:12088–107.
38. Su Y, Xu J, Shi Q, Yu L, Cai T. Polymorphism of griseofulvin: concomitant crystallization from the melt and a single crystal structure of a metastable polymorph with anomalously large thermal expansion. Chem Commun. 2018;54:358–61.
39. Su Y, Yu L, Cai T. Enhanced crystal nucleation in glass-forming liquids by tensile fracture in the glassy state. Crys Growth Des. 2018;19:40–4.
40. Ou X, Li X, Rong H, Yu L, Lu M. A general method for cultivating single crystals from melt microdroplets. Chem Commun. 2020;56:9950–3.
41. Hédoux A. Recent developments in the Raman and infrared investigations of amorphous pharmaceuticals and protein formulations: A review. Adv Drug Deliv Rev. 2016;100:133–46.
42. Chen Z, Liu Z, Qian F. Crystallization of bifonazole and acetaminophen within the matrix of semicrystalline, PEO–PPO–PEO triblock copolymers. Mol Pharm. 2015;12:590–9.
43. Potter CB, Davis MT, Albadarin AB, Walker GM. Investigation of the dependence of the Flory-Huggins interaction parameter on temperature and composition in a drug-polymer system. Mol Pharm. 2018;15:5327–35.
44. Tian Y, Booth J, Meehan E, Jones DS, Li S, Andrews GP. Construction of drug-polymer thermodynamic phase diagrams using Flory-Huggins interaction theory: identifying the relevance of temperature and drug weight fraction to phase separation within solid dispersions. Mol Pharm. 2013;10:236–48.
45. Shi Q, Zhang C, Su Y, Zhang J, Zhou D, Cai T. Acceleration of crystal growth of amorphous griseofulvin by low-concentration poly(ethylene oxide): Aspects of crystallization kinetics and molecular mobility. Mol Pharm. 2017;14:2262–72.
46. Kestur US, Taylor LS. Evaluation of the crystal growth rate of felodipine polymorphs in the presence and absence of additives as a function of temperature. Cryst Growth Des. 2013;13:4349–54.
47. Trasi NS, Taylor LS. Effect of polymers on nucleation and crystal growth of amorphous acetaminophen. CrystEngComm. 2012;14:5188–97.

48. Cui X, Shtukenberg AG, Freudenthal J, Nichols S, Kahr B. Circular birefringence of banded spherulites. J Am Chem Soc. 2014;136:5481–90.
49. Shtukenberg A, Freundenthal J, Gunn E, Yu L, Kahr B. Glass-crystal growth mode for testosterone propionate. Cryst Growth Des. 2011;11:4458–62.
50. Zhang Z, Wang Y, Huang X, Ding S, Chen K, Wang N, Hao H. Formation and growth mechanism of ceftezole sodium monohydrate ring-banded spherulites. Cryst Growth Des. 2021;21:5967–75.
51. Yang Y, Shtukenberg AG, Zhou H, Ruzie C, Geerts YH, Lee SS, Kahr B. Coherence in polycrystalline thin films of twisted molecular crystals. Chem Mater. 2024;36:881–91.